

1 **Strengthened causal connections between the MJO and the North Atlantic**  
2 **with climate warming**

3  
4 Savini M. Samarasinghe<sup>3,4</sup>, Charlotte Connolly<sup>1</sup>, Elizabeth A. Barnes<sup>1</sup>, Imme Ebert-Uphoff<sup>2,3</sup>  
5 and Lantao Sun<sup>1</sup>

6  
7 <sup>1</sup>Department of Atmospheric Science, Colorado State University, Fort Collins, CO

8 <sup>2</sup>Cooperative Institute for Research in the Atmosphere, Colorado State University, Fort Collins,  
9 CO

10 <sup>3</sup>Department of Electrical and Computer Engineering, Colorado State University, Fort Collins,  
11 CO

12 <sup>4</sup>Department of Geophysics, Colorado School of Mines, Golden, CO

13

14

15 Corresponding author: Savini M. Samarasinghe (samarasinghe@mines.edu)

16

17

18 **Key Points:**

- 19 ● CESM2-WACCM captures both the stratospheric and tropospheric pathways connecting  
20 the MJO to the North Atlantic  
21 ● MJO teleconnections to the North Atlantic strengthen in the future under SSP585 forcing  
22 ● The strengthening of the MJO-NAO connection is due to the tropospheric pathway while  
23 the stratospheric pathway changes very little

24 **Abstract**

25 While the Madden Julian Oscillation (MJO) is known to influence the midlatitude circulation  
26 and its predictability on subseasonal-to-seasonal (S2S) timescales, little is known how this  
27 connection may change with anthropogenic warming. This study investigates changes in the  
28 causal pathways between the MJO and the North Atlantic Oscillation (NAO) within historical  
29 and SSP585 simulations of the CESM2-WACCM coupled climate model. Two data-driven  
30 approaches are employed, namely, the STRIPES index and graphical causal models. These  
31 approaches collectively indicate that the MJO's influence on the North Atlantic strengthens in  
32 the future, consistent with an extended jet-stream. In addition, the graphical causal models allow  
33 us to distinguish the causal pathways associated with the teleconnections. While both a  
34 stratospheric and tropospheric pathway connect the MJO to the North Atlantic in CESM2-  
35 WACCM, the strengthening of the MJO-NAO causal connection over the 21st century is shown  
36 to be due exclusively to teleconnections via the tropospheric pathway.

37

38 **Plain Language Summary**

39 Climate models are useful tools for obtaining better understanding of the complex mechanisms  
40 that govern Earth's climate, as well as better understanding of the impacts of climate change.  
41 This study focuses on using the Community Earth System Model 2 - Whole Atmosphere  
42 Community Climate Model (CESM2-WACCM) climate model output along with several data-  
43 driven approaches to gain such insights. We focus specifically on the Madden Julian Oscillation  
44 (MJO), an atmospheric phenomenon of regions of stormy air and dry air that slowly progresses  
45 around the globe in the tropics. The MJO is well known to have an influence on the weather and  
46 climate of many parts of the world, including the North Atlantic. Our study finds that the  
47 CESM2-WACCM climate model correctly simulates connections between the MJO and the  
48 North Atlantic and that this influence strengthens over the 21<sup>st</sup> century. These insights have  
49 important implications for understanding how our ability to forecast weather over Europe and  
50 eastern North America may change in the coming decades.

## 51 **1 Introduction**

52 The Madden-Julian oscillation (MJO) has long been identified as an important source of  
53 midlatitude weather predictability on subseasonal-to-seasonal timescales (S2S; approximately 2  
54 weeks to 3 months) via its teleconnections to higher latitudes. Tropical convection associated  
55 with the MJO slowly propagates eastward in a quasi-periodic manner, taking approximately 20-  
56 90 days to circumnavigate the globe and complete a cycle (Madden and Julian 1971, 1972;  
57 Zhang 2013). MJO activity can excite Rossby waves which propagate out of the tropics and into  
58 the midlatitudes, modifying the large-scale circulation and weather patterns. Because it can take  
59 10-15 days for the teleconnection to reach the midlatitudes, knowing the state of the MJO today  
60 can provide information about the evolution of the midlatitude flow in the coming weeks. In fact,  
61 multiple studies have demonstrated that the MJO can be used to make skillful forecasts of  
62 weather up to 5 weeks in advance across the Northern Hemisphere (Cassou 2008; Baggett et al.  
63 2017; Mundhenk et al. 2018; Nardi et al. 2020).

64  
65 While much is known about the MJO and its role in S2S weather prediction, there is substantial  
66 uncertainty about how MJO teleconnections may be responding, and will continue to respond, to  
67 anthropogenic climate change. Changes can manifest through a combination of changes to the  
68 MJO itself and changes to the source and propagation of the Rossby waves into midlatitudes.  
69 Focusing first on changes to the MJO itself, Bui and Maloney (2019) show that ratio of MJO-  
70 induced circulation to precipitation in CMIP5 climate models decreases as the climate warms,  
71 and Hsiao et al. (2020) provide evidence that these changes may already be detectable in the  
72 observations. These results are important as they suggest that MJO teleconnections, which are  
73 directly excited by the MJO divergent circulation, may weaken as the climate warms (Wolding et  
74 al. 2017; Maloney et al. 2019). Thus, the response of the MJO alone to climate warming suggests  
75 that skill provided by the MJO could disappear in the coming decades.

76  
77 Changes in Rossby wave propagation with climate warming are also expected to impact MJO  
78 teleconnections. Zhou et al (2020) investigated changes in MJO teleconnections within  
79 CMIP5/CMIP6 climate models and demonstrated a robust increase in teleconnections to the west  
80 coast of the United States. Their reasoning was that the robust extension of the North Pacific jet-  
81 stream changes the Rossby wave propagation paths, acting to shift the teleconnection centers  
82 eastward to more directly impact the U.S. west coast. How Rossby wave propagation to the  
83 North Atlantic and Europe may change is perhaps more complicated. MJO teleconnections to  
84 these regions are known to be dynamically driven by two different pathways, a direct  
85 tropospheric pathway and an indirect stratospheric pathway (Barnes et al. 2019). The  
86 tropospheric pathway is communicated via tropospheric propagation of Rossby waves from the  
87 MJO region to the midlatitudes, which takes approximately 10-15 days (L'Heureux and Higgins  
88 2008; Cassou 2008; Lin et al. 2009). The stratospheric pathway instead involves MJO-excited  
89 Rossby waves propagating up into the stratosphere and disturbing the stratospheric polar vortex  
90 (a time lag of approximately 15-30 days) (Weare 2010; Garfinkel et al. 2012, 2014; Kang and

91 Tziperman 2018; Barnes et al. 2019). It is the signal from the disrupted polar vortex which then  
92 propagates downward into the troposphere, impacting the North Atlantic circulation (e.g.  
93 Baldwin and Dunkerton 2001; Garfinkel et al. 2014; Kidston et al. 2015; Charlton-Perez et al.  
94 2018). These multiple pathways connecting the MJO to the North Atlantic suggest that changes  
95 in teleconnection strength could come about due to changes in Rossby wave propagation through  
96 the troposphere, through the stratosphere, stratosphere-troposphere coupling, or changes to the  
97 MJO itself.

98  
99 Here, we investigate how MJO teleconnections to the North Atlantic may change under  
100 anthropogenic climate change using 3 historical and 5 SSP585 simulations of the Community  
101 Earth System Model 2 - Whole Atmosphere Community Climate Model (CESM2-WACCM).  
102 We invoke two data-driven approaches, namely, the STRIPES index and graphical causal models  
103 to quantify MJO teleconnection pathways within CESM2-WACCM and how they may evolve  
104 with climate warming. These approaches collectively indicate that the MJO's influence on the  
105 North Atlantic strengthens in the future and that this change is due exclusively to the  
106 tropospheric pathway.

107

## 108 **2 Data**

### 109 *2.1 CESM2-WACCM simulations*

110 We analyze simulations from the latest generation of the Community Earth System Model  
111 (CESM2; Danabasoglu et al. 2020) with the “high-top” atmospheric model. This coupled  
112 climate model is composed of the Whole Atmosphere Community Climate Model version 6  
113 (WACCM; Gettelman et al. 2019), Parallel Ocean Program Version 2 (POP2), CICE version  
114 5.1.2, Community Land Model Version 5 as well as the components of land ice and coupling.  
115 WACCM6 uses a nominal  $1^\circ$  ( $1.25^\circ$  longitude and  $0.95^\circ$  latitude) horizontal resolution  
116 configuration with 70 vertical levels with the model top of  $4.5 \times 10^{-6}$  hPa (about 130 km).  
117 Changes in CESM2 compared to CESM1 (Hurrell et al. 2013) have resulted in improved  
118 historical simulations including major reduction in low-latitude precipitation, and better  
119 representation of the MJO and extratropical atmospheric circulation, making it an ideal model for  
120 our study (Danabasoglu et al. 2020; Simpson et al. 2020; Ahn et al. 2020). This study was also  
121 repeated for the “low top” version - CESM2 - and the general conclusions remain the same as  
122 those found for CESM2-WACCM (see Supp. Fig. 6,7).

123

124 We analyze data from ensemble members 1, 2, 3 with historical (1850-2014) forcing and  
125 ensemble members 1, 2, 3, 4, 5 with SSP585 (2015-2099) forcing. SSP585 represents the high  
126 range of possible futures and exhibits an end of century radiative forcing of  $8.5 \text{ W/m}^2$  (O'Neill  
127 et al. 2016). We focus on daily sea-level pressure, zonal wind at 850 hPa, 250 hPa, and 50 hPa,  
128 and precipitation. All fields are re-gridded to a  $2^\circ$  by  $2^\circ$  grid prior to analysis to speed-up  
129 computation and reduce data storage. While we center our focus on winter subseasonal

130 variability in December, January and February (DJF), the causal inference approach uses time-  
131 shifted/lagged variables that are allowed to extend to November and March as appropriate.

132

## 133 *2.2 Climate indices*

134 When computing each of the three climate indices below (i.e. MJO, VORTEX and NAO) every  
135 ensemble member and 40-year period are treated completely separately to ensure that the  
136 analysis is agnostic to the number of ensemble members available. Prior to any analysis, we  
137 remove the 3rd order polynomial trend from each calendar day for each grid point for each field,  
138 which removes both the trend over the period and the seasonal cycle. This is done to ensure that  
139 all climate indices reflect subseasonal variability, rather than a long-term trend in the mean  
140 fields. Ensemble-averages are only performed as a final step prior to plotting the results.

141

142 The North Atlantic Oscillation (NAO) is defined as the leading empirical orthogonal function  
143 (EOF) of area-weighted monthly-mean SLP anomalies over the region 25N-90N, 90W-30E. The  
144 principal components are defined such that a positive value refers to a positive NAO state (low  
145 pressure over the poles and high pressure over the mid-North Atlantic) and have been  
146 standardized to have a mean of zero and standard deviation of one in Dec.-Feb. NAO sea-level  
147 pressure composites from CESM2-WACCM are provided in Supp. Figure 1.

148

149 The state of the stratospheric polar vortex (VORTEX) is defined as the area-weighted average of  
150 anomalous daily 50 hPa zonal wind north of 65N (e.g. Baldwin et al. 1994; Charlton-Perez et al.  
151 2018; Barnes et al. 2019). The index is standardized by subtracting the mean value over DJF and  
152 dividing by the standard deviation over DJF for each 40-year period.

153

154 The MJO is quantified by the real-time multivariate MJO index (RMM index; Wheeler and  
155 Hendon 2004) defined as the two leading EOFs of meridionally-averaged tropical (15S-15N)  
156 anomalous fields of 250 hPa and 850 hPa zonal wind and precipitation. We use model  
157 precipitation rather than outgoing longwave radiation (OLR) as is convention since precipitation  
158 is more directly simulated by the model. Numerous climate model diagnostics studies use  
159 precipitation anomalies to assess MJO simulation skill, and model MJO skill metrics are higher  
160 when evaluated with precipitation compared to OLR (Ahn et al. 2017, 2020). In addition to  
161 removing the seasonal cycle, we subtract the previous 120-day running mean from each field for  
162 each gridpoint to remove any low-frequency modes of variability prior to EOF analysis. Each of  
163 the three fields are also standardized by removing the mean and dividing by the standard  
164 deviation over all seasons. Supp. Figure 2 shows the structure of the two leading EOFs in the  
165 historical and future periods and the historical EOFs compare well with those from observations  
166 (Wheeler and Hendon 2004). The two leading principal components (denoted as RMM1 and  
167 RMM2) are standardized to have mean of zero and standard deviation of one. The different  
168 phases of the MJO are then defined by the phase space of RMM1 and RMM2 in the conventional

169 way (Wheeler and Hendon 2004). We define an MJO event as any day where the MJO amplitude  
170 ( $\sqrt{RMM1^2 + RMM2^2}$ ) exceeds 1.0.

171  
172 As has been documented previously, under a warming climate the MJO EOFs shift eastward  
173 compared to the historical period in CESM2-WACCM due to the eastward extension of tropical  
174 Pacific warm sea-surface temperatures (Subramanian et al. 2014; Maloney et al. 2019; Zhou et  
175 al. 2020). Due to the shift in the EOFs with warming, we are careful when determining the sign  
176 and convention of RMM1 and RMM2 by maximizing the spatial correlation of EOF1 and EOF2  
177 with their historical counterparts.

178

### 179 **3 Data-driven approaches**

#### 180 *3.1 STRIPES Index*

181 The STRIPES (Sensitivity to the Remote Influence of Periodic EventS) index is designed to  
182 capture regional sensitivities to the remote influence of periodic events in a single number  
183 (Jenney et al. 2019). Here, we use the STRIPES index to quantify the impacts of the MJO (i.e.  
184 magnitude and consistency) on the midlatitude circulation at each midlatitude gridpoint.  
185 Specifically, we compute the SLP anomalies 0-35 days following every MJO event of a  
186 particular phase. If there is a strong influence of the MJO on that grid point, a tilted stripe will be  
187 present in a plot of SLP anomalies as a function of lag (0-35 days) and MJO phase (1-8). A  
188 variance calculation of these tilted anomalies produces the STRIPES value, where we focus on  
189 tilts that correspond to MJO propagation speeds of 5-7 days per phase. A detailed explanation  
190 and visualization of the STRIPES index calculation can be found in Jenney et al. (2019). A  
191 higher STRIPES value indicates a larger variance in SLP anomalies, and thus, larger remote  
192 influence of the propagating MJO. The ensemble-mean STRIPES index is computed as the  
193 average STRIPES value across ensemble members.

194

#### 195 *3.2 Graphical causal models*

196 Graphical causal models based on Bayesian networks have been successfully used in climate  
197 science to gain insights into atmospheric teleconnections (Ebert-Uphoff and Deng 2012;  
198 Kretschmer et al. 2016; Runge et al. 2019) and cross-scale interactions (Samarasinghe et al.  
199 2020), as well as for climate model evaluation (Nowack et al. 2020; Vázquez-Patiño et al. 2020).  
200 These approaches provide a compact visual representation of the salient interactions between a  
201 set of random variables by representing the variables as nodes of a Directed Acyclic Graph  
202 (DAG) and the direct causal relationships between them as arrows/directed edges. In this study  
203 we use a temporal extension (Chu et al. 2005; Ebert-Uphoff and Deng 2012) of the “PC-stable”  
204 algorithm (Colombo and Maathuis 2014; Spirtes et al. 2000) to efficiently derive a DAG from  
205 our model data. However, the interactions identified from this data-driven approach (as opposed  
206 to targeted simulations) are only *potential* interactions and are *not guaranteed* to be true causal  
207 interactions due to reasons such as hidden common causes. Nevertheless, this method provides  
208 several advantages over traditional techniques such as correlation analysis and lagged regression

209 by allowing one to easily distinguish direct interactions from indirect ones in a multivariate  
 210 setting while still accounting for the memory and feedbacks. See Ebert-Uphoff and Deng (2012)  
 211 and Samarasinghe (2020), for explanations. Barnes et al. (2019) demonstrated that this causal  
 212 model approach is capable of distinguishing between the tropospheric and stratospheric pathway  
 213 of MJO teleconnections to the North Atlantic within observations.

214 In this study, we derive a temporal DAG by representing the MJO, NAO, and the polar vortex  
 215 and lagged copies of these variables as separate nodes in a graph. The PC-stable algorithm starts  
 216 with a fully connected undirected graph initially assuming interactions between every pair of  
 217 variables, however, instantaneous connections are not allowed. Next, a conditional independence  
 218 test is used to iteratively disprove the assumed interactions. A pair of variables X and Y cannot  
 219 have a direct causal connection if they are conditionally independent given any subset of nodes S  
 220 (excluding X and Y) in the graph. If there is such a subset S, the edge between X and Y is  
 221 eliminated. We statistically test for zero partial correlation using Fisher’s Z-test as the  
 222 conditional independence test with a confidence level alpha of 0.005, thus focusing on the  
 223 average linear dependencies between variables. Finally, we orient the edges such that the  
 224 interactions are from the past to the future. Our temporal model uses 12 lags each for the MJO,  
 225 NAO and VORTEX variables with each lag being 5 days apart. We discard one time slice to deal  
 226 with initialization issues following Ebert-Uphoff and Deng (2012).

227 To understand how the MJO-NAO teleconnection changes over time, we investigate the  
 228 interactions identified by PC-stable for each 40-year long window in the historical and future  
 229 periods, with a 10-year shift between adjacent windows. Prior to the causal analysis, we detrend  
 230 each 40-year-long NAO and VORTEX time series by removing a first-order polynomial fit of  
 231 each calendar day and then smooth the data with a 5-day, backward-looking average. We define  
 232 binary indicator variables for each MJO phase. These variables indicate an MJO event happening  
 233 in the phase of interest with ‘1’, and ‘0’ otherwise. Unless otherwise noted, we conduct the  
 234 causal analysis for pairs of phases to increase sample sizes for each group (i.e. phases 2/3, 4/5,  
 235 6/7, 8/1).

236 For each ensemble member, we derive a separate DAG for each 40-year window. We quantify  
 237 the robustness of each potential causal connection via the “temporal consistency fraction” (tcf)  
 238 defined below.

$$239 \quad tcf_{\text{member } i, X \rightarrow Y \text{ at lag } D} = \frac{\# \text{ of times the interaction } X \xrightarrow{D} Y \text{ is in DAG}_i}{\max \# \text{ of times the interaction } X \xrightarrow{D} Y \text{ can occur in DAG}_i}$$

240 A fraction closer to 1.0 indicates that the interaction is consistently repeating in the temporal  
 241 model, and thus, robust within that time frame. Figure 3a shows a summary of the potential  
 242 causal interactions learned by PC-stable that have a tcf of 0.6 or greater for a sample 40-year  
 243 window of an ensemble member. We average this fraction over the ensemble members as a

244 metric to distinguish robust causal signals in the CESM2-WACCM model while accounting for  
245 internal variability. See Supp. Fig. 5 for details.

#### 246 **4 Results**

247 Figure 1 compares composites of anomalous sea-level pressure 15 days following MJO phase 7  
248 events between the historical (1850-1889) and future (2055-2094) period for all ensemble  
249 members. The SLP teleconnection pattern over the North Atlantic compares well with that  
250 observed following MJO phase 7 (Henderson et al. 2016; their Fig. 6), and represents the  
251 negative phase of the NAO (e.g. Hurrell 1995). SLP anomalies increase substantially between  
252 the historical and future period, suggesting either stronger or more consistent teleconnections  
253 between the MJO and North Atlantic under future climate warming. This strengthening is also  
254 present when the two periods are more evenly compared using three ensemble members each  
255 (Supp. Fig. 3) or when alternative lags are considered (Supp. Fig. 4).

256  
257 Figure 1 displays results for MJO phase 7 only, however, since the MJO EOFs shift with  
258 warming (and thus the phase definitions may too), one would like to know whether the  
259 teleconnections are indeed strengthening, or just shifting to a different MJO phase. To quantify  
260 the extent to which MJO teleconnections to the NAO *over all MJO phases* strengthen under  
261 SSP585, we plot the ensemble-mean STRIPES index for the two periods, and their difference, in  
262 Figure 2. Larger STRIPES values imply a larger influence of the MJO on the SLP anomalies  
263 there, taking into consideration all phases. The well-known MJO-teleconnection hotspots over  
264 the Gulf of Alaska and the North Atlantic are identifiable in both periods (Figure 2a,b) (e.g.  
265 Cassou 2008; Lin et al. 2009; Mori 2008). While the location of the teleconnection hotspots  
266 appear similar between the two periods, the magnitude of the STRIPES index over these hotspots  
267 increases substantially by the end of the 21st century under SSP585 compared to the early  
268 historical period (Figure 2c,d). That is, consistent with Figure 1, the STRIPES analysis quantifies  
269 a strengthening of the MJO teleconnections with warming, with the largest changes occurring  
270 over the Gulf of Alaska and the North Atlantic. While the focus of this study is on the North  
271 Atlantic, we return to the North Pacific response in Section 5.

272  
273 Our results support a strengthening of the teleconnection between the MJO and NAO under  
274 SSP585, however, the methodology thus far does not allow us to distinguish between the  
275 tropospheric and stratospheric pathways. To do this, we compute graphical causal models of the  
276 MJO, stratospheric polar vortex, and the NAO (see Section 3 for methodology). An example  
277 result is shown in Figure 3a for MJO phases 6/7 within a single ensemble member for the 1970-  
278 2009 period. Arrows denote potential causal connections between climate phenomena, pointing  
279 in the direction of cause to effect, and numbers denote the time lag of the connection in days.  
280 Arrows that loop back on themselves signify temporal autocorrelation. The graphical model in  
281 Figure 3a demonstrates that CESM2-WACCM simulates a direct tropospheric pathway from the  
282 MJO to the NAO with a time lag of approximately 15 days following phases 6/7. Furthermore,  
283 CESM2-WACCM also simulates a stratospheric pathway, evidenced by a connection between

284 the MJO and the VORTEX (time lag of 15 days) and then VORTEX to the NAO (time lag of 5  
285 days), resulting in a total time lag of 20 days or so. These connections and time lags are  
286 consistent with what is observed over 1979-2016 in reanalyses (Barnes et al. 2019).  
287

288 Graphs such as that shown in Figure 3a are computed for each 40-year period for each ensemble  
289 member for each pair of MJO phases. We summarize the results by computing the temporal  
290 consistency fraction (see Section 3) of each connection for each time lag, period and ensemble  
291 member, and then average across members. In doing so, we obtain an estimate of the consistency  
292 of the causal connection for lags of 5-40 days as a function of time, as shown in Figure 3b.  
293 Colored lines denote different causal connections (i.e. arrows in Figure 3a) and it is clear that the  
294 direct, tropospheric MJO→NAO connection (pink) substantially strengthens over the 20th and  
295 21st centuries. The stratospheric pathway, however, shows no evidence of strengthening over the  
296 21st century, with the MJO→VORTEX connection (purple) weakening mid-20th century and  
297 then returning to 1800 values, and the VORTEX→NAO connection (brown) remaining constant  
298 over the entire 250 years. That is, the causal models suggest that the changes in MJO  
299 teleconnection strength under SSP585 forcings can be attributed exclusively to the tropospheric  
300 pathway, with the stratospheric pathway remaining largely unchanged.  
301

302 Both the MJO→NAO and MJO→VORTEX causal connections show pronounced increases in  
303 their temporal consistency fractions in the middle of the 20th century (Figure 3b, pink and purple  
304 lines). This mid-century peak may be related to the strong impact of aerosols on the North  
305 Atlantic during this period (Booth et al. 2012). While this explanation may explain the  
306 enhancement of the MJO→NAO causal connection, it is less clear for the MJO→VORTEX. We  
307 speculate that it is possible that the North Atlantic aerosol forcing, or the Multidecadal Atlantic  
308 Variability (AMV) associated with it, also impacted the stratospheric polar vortex (e.g. Omrani  
309 et al. 2014) and thus its connection to the MJO. Additional analysis is required to determine  
310 whether this is actually the case.  
311

312 The STRIPES and graphical causal model analyses provide strong evidence of a strengthening of  
313 the tropospheric MJO to NAO teleconnection under climate warming within CESM2-WACCM.  
314 At a fundamental level, this could be brought about by (1) a strengthening of the Rossby wave  
315 source in the tropics, (2) a strengthening of the wave propagation within the midlatitudes, or  
316 both. While a systematic study of the relative importance of each of these mechanisms is outside  
317 the scope of this study, Zhou et al. (2020) suggest that the extension of the North Pacific jet with  
318 warming can explain shifts in MJO teleconnections over the western United States in CMIP5 and  
319 CMIP6 simulations. We also find a robust extension of the North Pacific and North Atlantic jet-  
320 streams within CESM2-WACCM (contours in Figure 2c). This extension of the jet-stream from  
321 the North Pacific, across North America, and into Europe may enhance the waveguide,  
322 supporting Rossby wave propagation from the tropics to the North Atlantic (mechanism #2

323 above). In fact, changes in the STRIPES index align well with the extensions to the jet,  
324 especially over the North Atlantic basin (Figure 2c).

325  
326 On the other hand, enhancement and shift of the Rossby wave source, for example, through  
327 changes in the magnitude and location of MJO heating, could also be at play. While Zhou et al.  
328 (2020) focused predominantly on the shift of the MJO teleconnection pattern, their linear  
329 baroclinic model experiments suggest that changes in MJO heating alone (a component of  
330 mechanism #1) may lead to stronger MJO teleconnections to the North Pacific (their Figure 2d).  
331 They do not show results for the North Atlantic. We do find that precipitation anomalies  
332 associated with the MJO increase under SSP585 in CESM2-WACCM (not shown), so further  
333 study is required to truly separate these two mechanisms within the simulations.

334

### 335 **5 Discussion and Conclusions**

336 This study is one of the first to provide evidence of strengthened MJO teleconnections to the  
337 North Atlantic under SSP585. This result is perhaps surprising, as recent studies have argued that  
338 robust increases in tropical static stability may lead to a weakening of MJO teleconnections as  
339 the climate system warms (Wolding et al. 2017; Maloney et al. 2019). MJO-to-North Atlantic  
340 teleconnections are known to occur via both a stratospheric and tropospheric pathway, and our  
341 graphical causal model approach allows us to clearly distinguish between the two. Thus, our  
342 results documenting a strengthening of the tropospheric pathway, and theoretical arguments  
343 suggesting weakening teleconnections via increased tropical static stability, may be reconciled if  
344 the strengthening of the tropospheric pathway is driven predominantly by changes to the  
345 waveguide outside of the tropics. To truly disentangle between these competing mechanisms,  
346 however, additional model experiments are likely necessary.

347

348 The focus of this study was MJO impacts on the North Atlantic, however, our hemispheric  
349 STRIPES analysis leaves open questions regarding a strengthening of the MJO-Gulf of Alaska  
350 teleconnection in CESM2-WACCM (Figure 2). A widening of the North Pacific jet-stream on its  
351 polar flank (Figure 2c) may reduce the Rossby wave reflection there and instead be more  
352 conducive to wave propagation and breaking (e.g. Ambrizzi et al. 1995). The mechanism behind  
353 this change is still not clear to the authors, given that one might expect the extended North  
354 Pacific jet to also shift the SLP anomaly eastward, something we do not see in Figures 1 or 2.  
355 Zhou et al. (2020) find a strengthening of the MJO-induced anomalies in the Gulf of Alaska  
356 region when only the MJO heating is modified to its future state in a linear baroclinic model, yet  
357 another possible reason for this response. Thus, further work is needed to understand this Gulf of  
358 Alaska response.

359

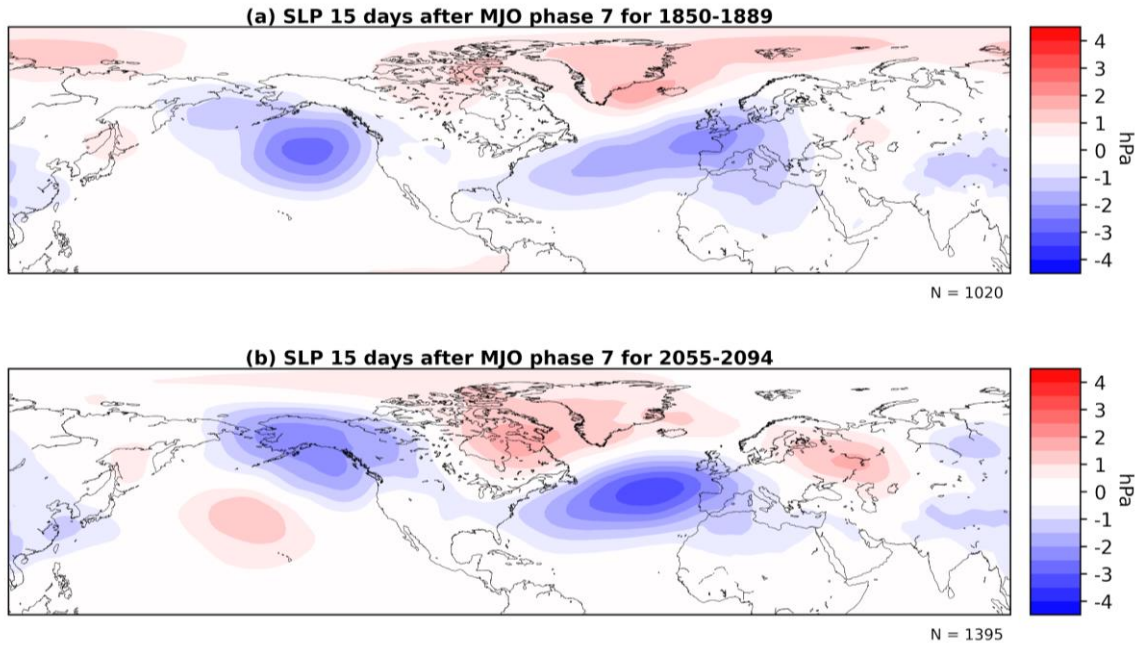
360 Our study employs two data-driven approaches for summarizing and quantifying MJO  
361 teleconnections to midlatitudes, and perhaps the methods used in this study are of as much  
362 interest as the results themselves. The STRIPES analysis allowed us to summarize many lag and

363 phase diagrams typically used to study MJO teleconnections, while the causal model approach  
364 helped disentangle the stratospheric and tropospheric pathways. Both methods provide a  
365 straightforward way to compare various teleconnection pathways and strengths within  
366 observations and climate models, as well as how the teleconnections may change with time.  
367

### 368 **Acknowledgements**

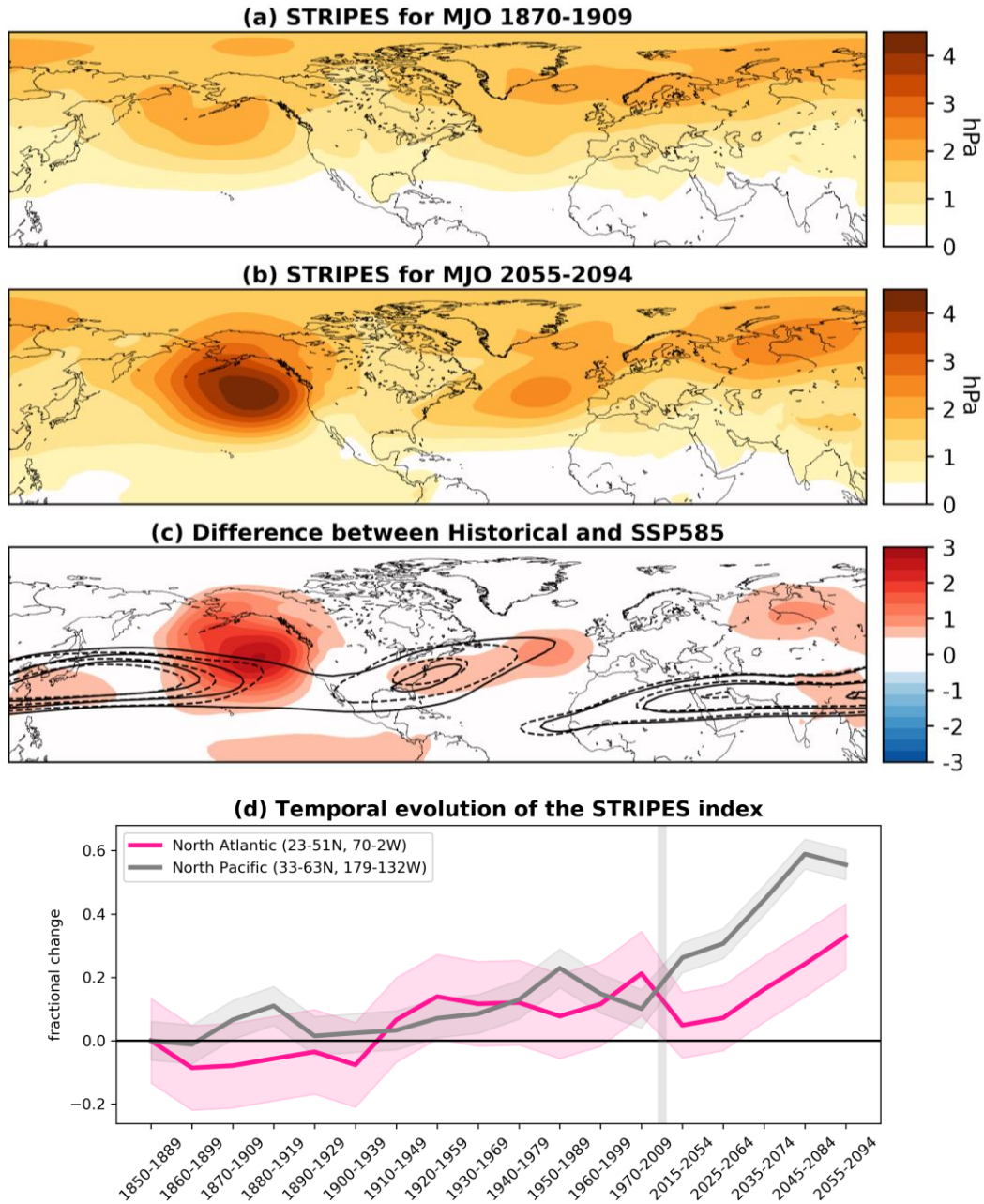
369 Work was supported by NSF CAREER AGS-1749261 under the Climate and Large-scale  
370 Dynamics program (SS, EB, CC, IE), NSF Award #1934668 of the Harnessing the Data  
371 Revolution (HDR) program (IE) and Jim Hurrell's presidential chair startup funding at CSU  
372 (LS). The CESM2-WACCM and CESM2 CMIP6 datasets are accessible on the Earth System  
373 Grid Federation website (CESM2-WACCM historical and SSP585:  
374 doi:10.22033/ESGF/CMIP6.10071, doi:10.22033/ESGF/CMIP6.10115; CESM2 historical and  
375 SSP585: doi:10.22033/ESGF/CMIP6.7627, doi:10.22033/ESGF/CMIP6.7768).

376  
377



378  
379  
380  
381  
382

**Figure 1:** Composite sea-level pressure anomalies 15 days following MJO phase 7 events averaged over ensemble members for the (a) historical (1850-1889; 3 simulations) and (b) future (2055-2094; 5 simulations) periods.



383

384

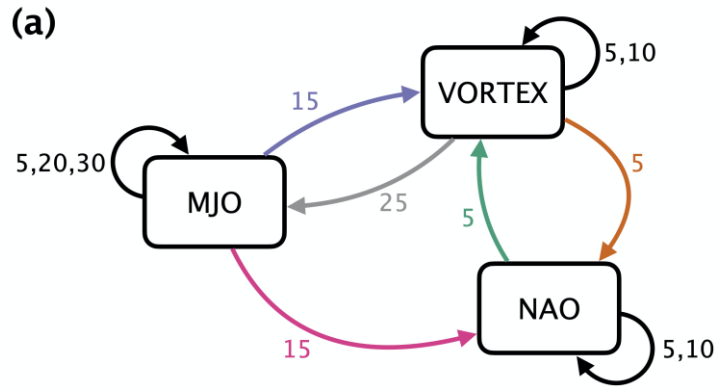
385 **Figure 2:** STRIPES values averaged over ensemble members for the (a) historical (1850-1889; 3  
 386 simulations) and (b) future (2055-2094; 5 simulations) periods, as well as their (c) difference.

387 Panel (d) displays time series of the regionally-averaged STRIPES, plotted in units of fractional  
 388 change from 1870-1909. Contours in (c) denote the ensemble-mean 250 hPa zonal winds  
 389 contoured at 30, 40 and 50 m/s, where dashed and solid lines denote the historical and future  
 390 periods respectively. Shading in (d) denotes the 90% confidence bounds on the sample mean  
 391 computed using the 20th century standard deviation across ensemble members. The gray vertical  
 392 bar denotes a break in the x-axis due to the transition from historical to SSP585 simulations.

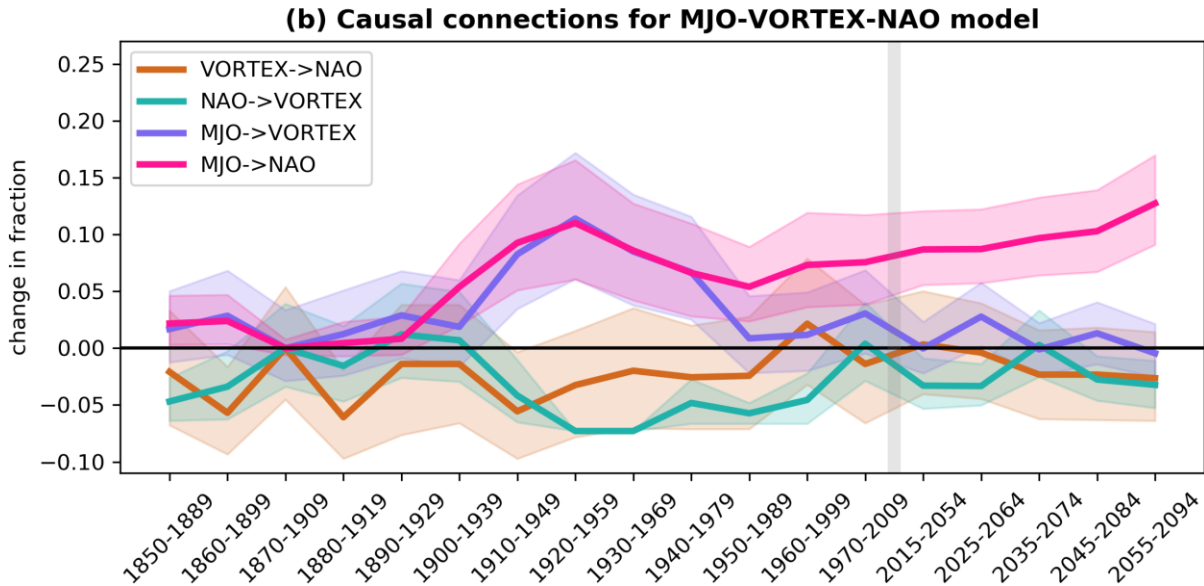
393

394

395



396  
397  
398



399  
400  
401  
402  
403  
404  
405  
406  
407  
408  
409  
410  
411  
412

**Figure 3:** (a) Example graphical causal model for MJO phases 6/7, the VORTEX, and the NAO based on results from historical ensemble member 3 over 1970-2009. (b) Fraction of causal connections relative to the ensemble-mean value in 1870-1909 for causal models of the MJO-VORTEX-NAO. Results are averaged over delays of 5-40 days and averaged over all MJO phases and ensemble members. Shading denotes 90% confidence bounds based on Monte Carlo resampling. The gray vertical bar denotes a break in the x-axis due to the transition from historical to SSP585 simulations.

413 **References**

- 414 Ahn, M., D. Kim, K. R. Sperber, I.-S. Kang, E. Maloney, D. Waliser, H. Hendon, and on behalf  
 415 of WGNE MJO Task Force, 2017: MJO simulation in CMIP5 climate models: MJO skill  
 416 metrics and process-oriented diagnosis. *Clim. Dyn.*, **49**, 4023–4045.
- 417 Ahn, M., D. Kim, D. Kang, J. Lee, K.R. Sperber, P.J. Gleckler, and Coauthors, 2020: MJO  
 418 Propagation Across the Maritime Continent: Are CMIP6 Models Better Than CMIP5  
 419 Models? *Geophys. Res. Lett.*, **47**, 741.
- 420 Ambrizzi, T., B. J. Hoskins, and H.-H. Hsu, 1995: Rossby Wave Propagation and  
 421 Teleconnection Patterns in the Austral Winter. *J. Atmos. Sci.*, **52**, 3661–3672.
- 422 Baggett, C. F., E. A. Barnes, E. D. Maloney, and B. D. Mundhenk, 2017: Advancing  
 423 atmospheric river forecasts into subseasonal-to-seasonal time scales. *Geophys. Res. Lett.*,  
 424 **44**, 2017GL074434.
- 425 Baldwin, M., and T. Dunkerton, 2001: Stratospheric harbingers of anomalous weather regimes.  
 426 *Science*, **294**, 581–584.
- 427 Baldwin, M. P., X. Cheng, and T. J. Dunkerton, 1994: Observed correlations between winter-  
 428 mean tropospheric and stratospheric circulation anomalies. *Geophys. Res. Lett.*, **21**, 1141–  
 429 1144.
- 430 Barnes, E. A., S. M. Samarasinghe, I. Ebert-Uphoff, and J. C. Furtado, 2019: Tropospheric and  
 431 Stratospheric Causal Pathways Between the MJO and NAO. *J. Geophys. Res. D: Atmos.*,  
 432 **124**, 9356–9371.
- 433 Booth, B. B. B., N. J. Dunstone, P. R. Halloran, T. Andrews, and N. Bellouin, 2012: Aerosols  
 434 implicated as a prime driver of twentieth-century North Atlantic climate variability. *Nature*,  
 435 **484**, 228–232.
- 436 Bui, H. X., and E. D. Maloney, 2019: Transient Response of MJO Precipitation and Circulation  
 437 to Greenhouse Gas Forcing. *Geophys. Res. Lett.*, **46**, 13546–13555.
- 438 Cassou, C., 2008: Intraseasonal interaction between the Madden-Julian Oscillation and the North  
 439 Atlantic Oscillation. *Nature*, **455**, 523–527.
- 440 Charlton-Perez, A. J., L. Ferranti, and R. W. Lee, 2018: The influence of the stratospheric state  
 441 on North Atlantic weather regimes: CHARLTON-PEREZ et al. *Q.J.R. Meteorol. Soc.*, **104**,  
 442 30937.
- 443 Chu, T., D. Danks, and C. Glymour, 2005: *Data Driven Methods for Nonlinear Granger*  
 444 *Causality: Climate Teleconnection Mechanisms*. Carnegie Mellon University,.
- 445 Colombo, D., and M. H. Maathuis, 2014: Order-independent constraint-based causal structure  
 446 learning. *J. Mach. Learn. Res.*,.

- 447 Danabasoglu, G., and Coauthors, 2020: The Community Earth System Model version 2  
448 (CESM2). *J. Adv. Model. Earth Syst.*, <https://doi.org/10.1029/2019MS001916>.
- 449 Ebert-Uphoff, I., and Y. Deng, 2012: Causal Discovery for Climate Research Using Graphical  
450 Models. *J. Clim.*, **25**, 5648–5665.
- 451 Garfinkel, C. I., S. B. Feldstein, D. W. Waugh, C. Yoo, and S. Lee, 2012: Observed connection  
452 between stratospheric sudden warmings and the Madden-Julian Oscillation. *Geophys. Res.  
453 Lett.*, **39**, L18807.
- 454 Garfinkel, C. I., J. J. Benedict, and E. D. Maloney, 2014: Impact of the MJO on the boreal winter  
455 extratropical circulation. *Geophys. Res. Lett.*, **41**, 6055–6062.
- 456 Gettelman, A., and Coauthors, 2019: The Whole Atmosphere Community Climate Model  
457 Version 6 (WACCM6). *J. Geophys. Res. D: Atmos.*, **124**, 12380–12403.
- 458 Henderson, S. A., E. D. Maloney, and E. A. Barnes, 2016: The Influence of the Madden–Julian  
459 Oscillation on Northern Hemisphere Winter Blocking. *J. Clim.*, **29**, 4597–4616.
- 460 Hsiao, W.-T., E. D. Maloney, and E. A. Barnes, 2020: Investigating Recent Changes in MJO  
461 Precipitation and Circulation in Two Reanalyses. *Earth and Space Science Open Archive*,.
- 462 Hurrell, J., 1995: Decadal trends in the north atlantic oscillation: regional temperatures and  
463 precipitation. *Science*, **269**, 676–679.
- 464 Hurrell, J. W., and Coauthors, 2013: The Community Earth System Model: A Framework for  
465 Collaborative Research. *Bull. Am. Meteorol. Soc.*, **94**, 1339–1360.
- 466 Jenney, A. M., D. A. Randall, and E. A. Barnes, 2019: Quantifying Regional Sensitivities to  
467 Periodic Events: Application to the MJO. *J. Geophys. Res. D: Atmos.*, **124**, 3671–3683.
- 468 Kang, W., and E. Tziperman, 2018: The MJO-SSW Teleconnection: Interaction Between MJO-  
469 Forced Waves and the Midlatitude Jet. *Geophys. Res. Lett.*, **45**, 4400–4409.
- 470 Kidston, J., A. A. Scaife, S. C. Hardiman, D. M. Mitchell, N. Butchart, M. P. Baldwin, and L. J.  
471 Gray, 2015: Stratospheric influence on tropospheric jet streams, storm tracks and surface  
472 weather. *Nat. Geosci.*, **8**, 433.
- 473 Kretschmer, M., D. Coumou, J. F. Donges, and J. Runge, 2016: Using Causal Effect Networks to  
474 Analyze Different Arctic Drivers of Midlatitude Winter Circulation. *J. Clim.*, **29**, 4069–  
475 4081.
- 476 L’Heureux, M. L., and R. W. Higgins, 2008: Boreal Winter Links between the Madden–Julian  
477 Oscillation and the Arctic Oscillation. *J. Clim.*, **21**, 3040–3050.
- 478 Lin, H., G. Brunet, and J. Derome, 2009: An Observed Connection between the North Atlantic  
479 Oscillation and the Madden–Julian Oscillation. *J. Clim.*, **22**, 364–380.

- 480 Madden, R. A., and P. R. Julian, 1971: Detection of a 40–50 Day Oscillation in the Zonal Wind  
481 in the Tropical Pacific. *J. Atmos. Sci.*, **28**, 702–708.
- 482 Madden, R. A., and P. R. Julian, 1972: Description of Global-Scale Circulation Cells in the  
483 Tropics with a 40–50 Day Period. *J. Atmos. Sci.*, **29**, 1109–1123.
- 484 Maloney, E. D., Á. F. Adames, and H. X. Bui, 2019: Madden–Julian oscillation changes under  
485 anthropogenic warming. *Nat. Clim. Chang.*, **9**, 26–33.
- 486 Mori, M., 2008: The Growth and Triggering Mechanisms of the PNA: A MJO–PNA Coherence.  
487 *J. Meteorol. Soc. Japan*, **86**, 213–236.
- 488 Mundhenk, B. D., E. A. Barnes, E. D. Maloney, and C. F. Baggett, 2018: Skillful empirical  
489 subseasonal prediction of landfalling atmospheric river activity using the Madden–Julian  
490 oscillation and quasi-biennial oscillation. *npj Climate and Atmospheric Science*, **1**, 7.
- 491 Nardi, K. M., C. F. Baggett, E. A. Barnes, E. D. Maloney, D. S. Harnos, and L. M. Ciasto, 2020:  
492 Skillful all-season S2S prediction of U.S. precipitation using the MJO and QBO. *Weather*  
493 *Forecasting*, <https://doi.org/10.1175/WAF-D-19-0232.1>.
- 494 Nowack, P., J. Runge, V. Eyring, and J. D. Haigh, 2020: Causal networks for climate model  
495 evaluation and constrained projections. *Nat. Commun.*, **11**, 1–11.
- 496 Omrani, N.-E., N. S. Keenlyside, J. Bader, and E. Manzini, 2014: Stratosphere key for  
497 wintertime atmospheric response to warm Atlantic decadal conditions. *Clim. Dyn.*, **42**, 649–  
498 663.
- 499 O’Neill, B. C., and Coauthors, 2016: The Scenario Model Intercomparison Project  
500 (ScenarioMIP) for CMIP6. *Geoscientific Model Development*, **9**, 3461–3482.
- 501 Runge, J., and Coauthors, 2019: Inferring causation from time series in Earth system sciences.  
502 *Nat. Commun.*, **10**, 2553.
- 503 Samarasinghe, S., Y. Deng, and I. Ebert-Uphoff, 2020: A Causality-Based View of the  
504 Interaction between Synoptic- and Planetary-Scale Atmospheric Disturbances. *J. Atmos.*  
505 *Sci.*, **77**, 925–941.
- 506 Samarasinghe, S. M., 2020: Causal Inference Using Observational Data-Case Studies in Climate  
507 Science. 2020-CSU Theses and Dissertations, Colorado State University, .
- 508 Simpson, I. R., and Coauthors, 2020: An Evaluation of the Large-Scale Atmospheric Circulation  
509 and Its Variability in CESM2 and Other CMIP Models. *J. Geophys. Res. D: Atmos.*, **125**,  
510 e2019MS001916.
- 511 Spirtes, P., C. Glymour, and R. Scheines, 2000: *Causation, Prediction, and Search, Second*  
512 *Edition*. MIT Press,.
- 513 Subramanian, A., M. Jochum, A. J. Miller, R. Neale, H. Seo, D. Waliser, and R. Murtugudde,

- 514           2014: The MJO and global warming: a study in CCSM4. *Clim. Dyn.*, **42**, 2019–2031.
- 515   Vázquez-Patiño, A., L. Campozano, D. Mendoza, and E. Samaniego, 2020: A causal flow  
516           approach for the evaluation of global climate models. *Int. J. Climatol.*, **40**, 4497–4517.
- 517   Weare, B. C., 2010: Extended Eliassen-Palm fluxes associated with the Madden-Julian  
518           oscillation in the stratosphere. *J. Geophys. Res.*, **115**, D24103.
- 519   Wheeler, M. C., and H. H. Hendon, 2004: An All-Season Real-Time Multivariate MJO Index:  
520           Development of an Index for Monitoring and Prediction. *Mon. Weather Rev.*, **132**, 1917–  
521           1932.
- 522   Wolding, B. O., E. D. Maloney, S. Henderson, and M. Branson, 2017: Climate change and the  
523           Madden-Julian Oscillation: A vertically resolved weak temperature gradient analysis. *J.*  
524           *Adv. Model. Earth Syst.*, **9**, 307–331.
- 525   Zhang, C., 2013: Madden–Julian Oscillation: Bridging Weather and Climate. *Bull. Am.*  
526           *Meteorol. Soc.*, **94**, 1849–1870.
- 527   Zhou, W., D. Yang, S.-P. Xie, and J. Ma, 2020: Amplified Madden–Julian oscillation impacts in  
528           the Pacific–North America region. *Nat. Clim. Chang.*, [https://doi.org/10.1038/s41558-020-](https://doi.org/10.1038/s41558-020-0814-0)  
529           0814-0.